Chalcogenide Letters Vol. 16, No. 2, February 2019, p. 49 - 55

PRISTINE AND Sm-DOPED ZnS QUANTUM DOTS: STRUCTURAL, OPTICAL, LUMINESCENCE, MAGNETIC, AND PHOTOCATALYTIC PROPERTIES

B. POORNAPRAKASH[a], U. CHALAPATHI[a], S.V. PRABHAKAR VTTIKUTI[b], M. S. PRATAP REDDY[c], S. H. PARK[a,*]

[a]*Department of Electronic Engineering, Yeungnam University, Gyeongsan 38541, South Korea*

[b]*School of Mechanical Engineering, Yeungnam University, Gyeongsan 38541, South Korea*

[c]*School of Electronics Engineering, Kyungpook National University, Daegu 41566, South Korea*

In this study, ZnS quantum dots (QDs) approximately 2.9 nm in size and doped with Sm (2 at%) were fabricated through the solvothermal route. Both pristine and Sm-doped ZnS QDs displayed a typical cubic structure as denoted by the X-ray diffraction pattern. The high-resolution transmission electron microscopy images of the suspensions display nearly spheroid-shaped QDs. The bandgap of the pristine and Sm-doped QDs was found to be 3.81 and 3.84 eV, respectively, which is greater than that of bulk ZnS (3.67 eV). The photoluminescence spectra of both QDs displayed a similar wide emission band, ranging from 350–500 nm, although the Sm-doped QDs exhibited higher fluorescence efficiency than the pristine ZnS. The magnetic analysis disclosed that the pristine QDs were diamagnetic whereas the Sm-doped QDs were paramagnetic at room temperature. The Sm-doped QDs exhibited a more effective photocatalytic activity during crystal violet dye degradation under UV-light irradiation compared to the pristine QDs. The engrossing properties of the Sm-doped ZnS QDs may be useful for applications in optoelectronics and photocatalysis.

(Received December 4, 2018; Accepted February 1, 2019)

Keywords: Zinc sulfide, Quantum dots, Optoelectronics, Photocatalysis

1. Introduction

Progress in materials technology over the past few decades calls for the utilization of II–VI wide bandgap semiconductor compounds for diverse applications. Among these, ZnS is an enticing candidate in the research community, as it exhibits unique properties that can be amended by doping with transition metals (TM) or rare earth (RE) ions. Doped ZnS quantum dots (QDs) have attracted increasing attention from current researchers investigating engineering and scientific applications in advanced optoelectronics, spintronics, and photocatalysis. A wide range of experimental results has been reported on the TM- and RE-doped ZnS nanoparticles, exhibiting interesting properties under sensible doping [1-6]. Particularly, the investigations on RE-doped ZnS are limited when compared to those of TM-doped ZnS in any form. However, RE doping can extend the optical absorption that impacts the bandgap of the semiconductor host and also renders it suitable for optoelectronics and photocatalysis applications. In addition, these candidates serve as a diluted magnetic semiconductor and may render them suitable for spintronic applications. The most recent results in optical, photocatalytic, and magnetic properties of RE-doped ZnS [7-10] have motivated our present investigation on RE-doped ZnS QDs. The preparation of RE-doped ZnS QDs is not easy using routine approaches, and demands particular synthesis conditions as mentioned in the experimental part in detail. In this study, we used the solvothermal method to

*Corresponding authors: sihyun_park@ynu.ac.kr

prepare the pristine and Sm-doped ZnS QDs. The structural, chemical, optical, luminescence, magnetic, and photocatalytic studies of the pristine and Sm-doped ZnS QDs were analyzed clearly.

2. Synthesis and characterization

Pristine and Sm (2 at%)-doped ZnS QDs were synthesized through the solvothermal route. Sigma–Aldrich chemicals were used in the present study. For the synthesis of pristine ZnS, 0.1 M of zinc nitrate (1.487 g) was added to 50 mL of ethanol and stirred vigorously for 30 min. Next, 0.1 M of sodium sulfide (1.2 g) solution was added drop wise to the above solution through a burette. Subsequently, 0.25 g of polyvinylpyrrolidone was added to the above suspension as a stabilizer and was transferred into an autoclave and maintained at 150 °C for 30 h. The acquired sample was maintained at 100 °C for one day. For the synthesis of Sm (2 at%)-doped ZnS, 0.1 M of zinc nitrate (1.427 g) and samarium nitrate (0.088 g) were added to 50 mL of ethanol and stirred for 30 min. The subsequent procedure is the same as that used to prepare pristine ZnS.

We used the same techniques, i.e., X-ray diffraction (XRD), high-resolution transmission electron microscopy (HRTEM), optical absorption, photoluminescence (PL), X-ray photoelectron spectroscopy (XPS), and vibrating sample magnetometer (VSM) as those used in our recently published articles [11-13]. The photocatalytic degradation (PCD) of the crystal violet dye was performed under UV light irradiation. The equipment used and PCD procedure are the same as those utilized in our recently published article [14]. However, we have used a different interval time (20 min) in the present study.

3. Results and discussion

3.1. X-ray diffraction analysis

The XRD patterns of pristine and Sm-doped ZnS QDs, as illustrated in Fig. 1, exhibit a cubic structure (JCPDS card No: 65-9585). The width of the XRD peaks stipulates the nanosize of the synthesized particles. A trivial shift towards higher angles and decreased peak intensity were observed in the ZnS QDs after Sm doping, indicating the effective substitution of Sm doping in the ZnS host as well as the reduction in the crystallinity. Additionally, the absence of further peaks corresponding to the foreign phases resulted in the impurity-free synthesized QDs. The crystallite sizes of the pristine as well as the Sm-doped ZnS QDs are 3.8 and 2.9 nm, respectively, calculated using Sherrers' equation [11, 12]. Recently, Bakhtkhosh et al. [6] reported the synthesis of ZnS nanoparticles approximately 22 nm in size that were doped with Sm (5 at%).

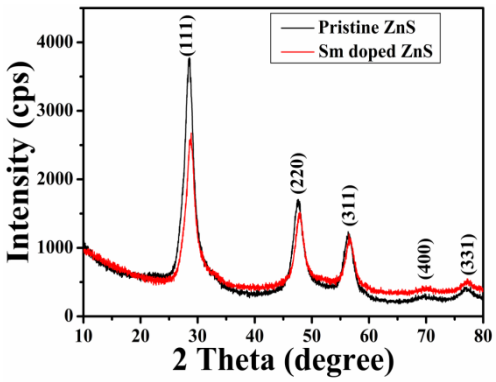

Fig. 1. XRD patterns of the pristine and Sm-doped ZnS QDs.

3.2. HRTEM analysis

HRTEM images of the (a) pristine and (b) Sm-doped ZnS QDs, are shown in Fig. 2, which

reveal the formation of slightly polydispersed and nearly spheroid-shaped particles. No change in the morphology was observed in the pristine ZnS after Sm doping. The assessed sizes of the prepared pristine and Sm-doped ZnS were 4.0 and 3.3 nm, respectively. The size of the Sm-doped ZnS QDs are smaller than their pristine counterparts suggests that the growth rate of the Sm-doped ZnS QDs was limited by the difference in the ionic radii of the dopant [15].

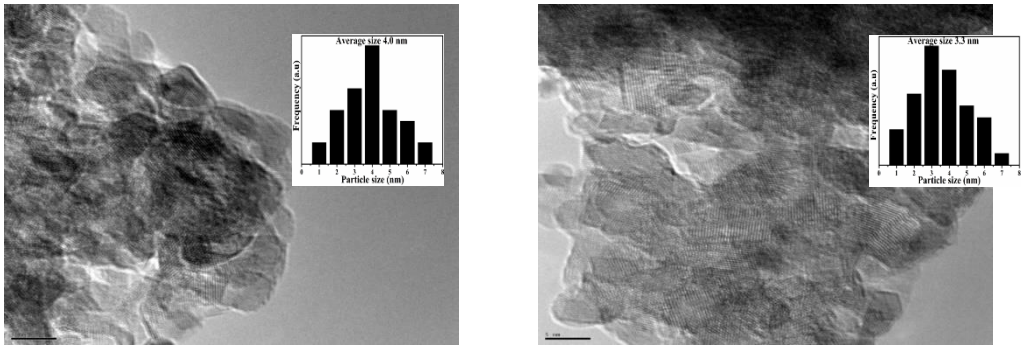

a) *b)*

Fig. 2. HRTEM images and (inset) size distribution histograms of (a) pristine and (b) Sm-doped ZnS QDs.

3.3. Optical and photoluminescence analysis

To obtain the optical bandgap of the pristine and Sm-doped ZnS QDs, the UV-Vis absorption spectra were recorded. The absorption spectra of the pristine and Sm-doped ZnS QDs are as shown in Fig. 3. The absorption peaks of the pristine and Sm-doped QDs are located at 326 and 322 nm, respectively, and are larger than those of the ZnS; this is due to the quantum confinement effect [14]. The bandgaps of the pristine and Sm-doped ZnS QDs were observed to be 3.80 and 3.84 eV, respectively. Furthermore, a slight blue shift was observed after Sm doping, owing to the decreased diameter of the QDs. Both HRTEM and XRD findings agree with the above results. The PL spectra of the pristine and Sm-doped ZnS QDs are exhibited in Fig. 4. The excitation wavelength of both samples is 300 nm. The PL spectra comprise a wide emission band ranging from 350–500 nm. However, the Sm-doped QDs exhibit higher fluorescence efficiency than the pristine ZnS. The wide emission band of these QDs may be due to the existence of shallow and deep traps beneath the conduction band induced by the surface defects of the synthesized QDs [16, 17]. The enhanced fluorescence efficiency may be correlated with both the HRTEM and XRD findings. A reduction in particle size engenders the increased surface defects, resulting in an enhancement in the fluorescence efficiency after Sm doping. This result suggests that Sm serves as a sensitizer [17]. Kushida et al. [18] reported that the wide fluorescence and excitation bands observed in the visible region might correspond to the transitions between the $^4f_6$ and $^4f_5$5d states of samarium (II) in the Sm-doped ZnS nanoparticles.

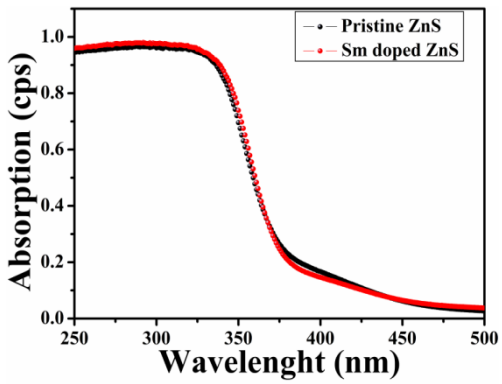

Fig. 3. Optical absorption spectra of pristine and Sm-doped ZnS QDs.

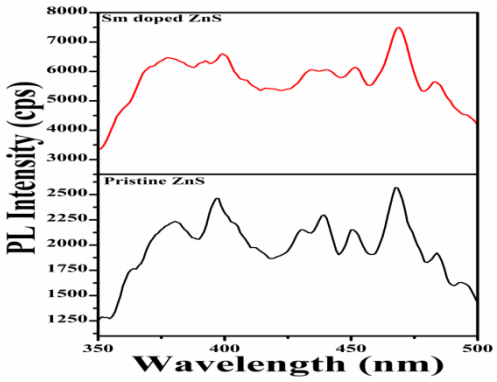

Fig. 4. PL spectra of pristine and Sm-doped ZnS QDs.

3.4 .Chemical analysis

To probe the oxidation state as well as the composition of Sm in the ZnS QDs, the XPS survey spectrum was recorded, as shown in Fig. 5. The elements Sm, Zn, and S are shown from the survey spectrum. The peaks due to Sm are located at 1082.98 and 1110.09 eV that correspond to the core levels Sm $3d_{3/2}$ and Sm $3d_{5/2}$, respectively, and confirm the existence of Sm in the ZnS as +3 [19]. The peaks due to Zn are located at 1022.38 and 1044.92 eV, corresponding to the binding energies of the Zn $2p_{3/2}$ and Zn $2p_{1/2}$, respectively, and affirming the divalent state of Zn. The peak of S is located at 161.88 eV and belongs to S 2p, indicating the -2 chemical state of the S. Moreover, no evidence of foreign phases corresponding to Sm was found in the Sm-doped ZnS QDs.

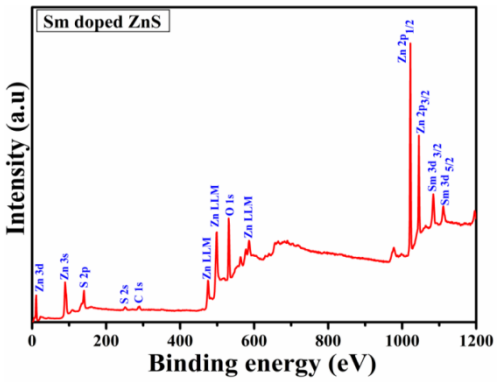

Fig. 5. XPS survey scan of Sm-doped ZnS QDs.

3.5. Magnetic analysis

The M–H curves for the pristine and Sm-doped ZnS QDs are as illustrated in Fig. 6. Typically, the pristine QDs exhibit diamagnetic character, whereas the Sm-doped QDs exhibit paramagnetic behavior at room temperature. The diamagnetic character of the pristine QDs is attributed to the deficiency of the unpaired electrons [7-9], while the paramagnetism of the Sm-doped QDs is due to the random distribution of the dopant ions in the host lattice engendering the creation of a frail interaction induced by the space among the Sm ions as well as the concentration [19].

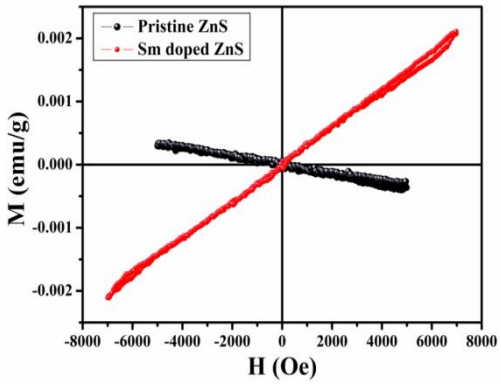

Fig. 6. M-H curves for pristine and Sm-doped ZnS QDs.

3.6. Photocatalytic properties

Fig. 7 shows the plot between C/C0 and time for the pristine and Sm-doped ZnS QDs. After 100 min of irradiation, 69.81% of crystal violet was degraded in the pristine QDs, while 80.11 % of crystal violet was degraded in the Sm-doped ZnS QDs. The PCD kinetics of the crystal violet solution with pristine and Sm-doped ZnS QDs under UV light illumination are displayed in Fig. 8. Correlating the improved PCD with the HRTEM, XRD, and PL results, we affirm that the size of the particles was reduced after Sm doping. A reduction in the particle size induces the increased surface defects, resulting in an increase in the defects and vacancies after Sm doping. These results strongly suggest that Sm-doped ZnS QDs are a favorable material for crystal violet degradation. More recently, Younes et al. [20] observed the enhanced photocatalytic activity in Sm-doped ZnS compared to that in undoped ZnS nanoparticles in reactive red 43 dye under visible light irradiation. Bakhtkhosh et al. [6] observed the higher PCD of direct blue 14 dye under UV light irradiation in Sm-doped ZnS than that in undoped ZnS nanoparticles prepared using the sonochemical method.

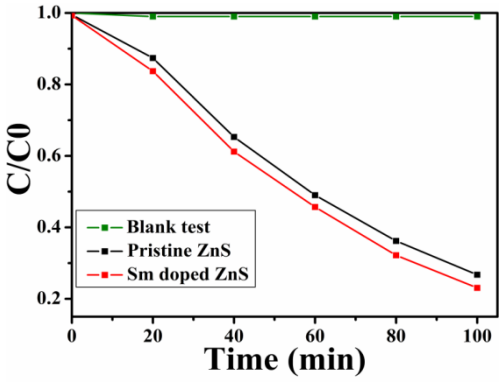

Fig. 7. Photocatalytic activities of the pristine and Sm-doped ZnS QDs.

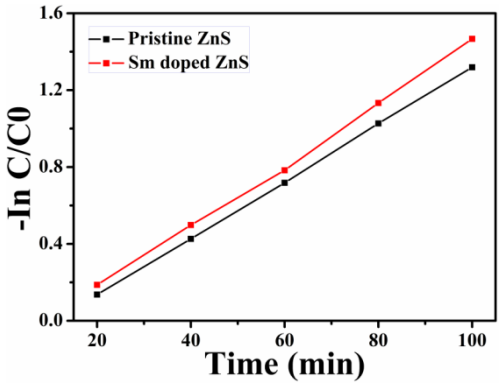

Fig. 8. Kinetic linear simulation of crystal violet photocatalytic degradation over the pristine and Sm-doped ZnS QDs.

4. Conclusions

We herein reported the structural, chemical, optical, luminescence, magnetic, and photocatalytic properties of pristine and Sm-doped ZnS QDs synthesized through the solvothermal method. All the synthesized samples exhibited a cubic phase as observed in the XRD pattern. Nearly spheroid-shaped particles were observed in the HRTEM images. The obtained bandgaps of these QDs were higher than those of bulk ZnS, a result of the quantum confinement effect. Both samples displayed the similar wide emission band from 350–500 nm; however, the PL intensity of the Sm-doped sample was higher than that of pristine ZnS. Diamagnetic and paramagnetic behaviors were exhibited by the pristine and Sm-doped ZnS QDs, respectively, at room temperature. The Sm-doped QDs demonstrated an increased photocatalytic activity compared to the pristine ZnS during the crystal violet dye degradation under UV-light irradiation. The engrossing properties of the Sm-doped ZnS QDs may be useful for optoelectronics and photocatalytic applications.

Acknowledgements

This research was supported by 2018 Research Supporting Program through the Hwasung Scholarship & Culture Foundation.

References

[1] D. Amaranatha Reddy, G. Murali, R. P. Vijayalakshmi, B. K. Reddy, Appl. Phys. A, **105** 119 (2011).
[2] Sanjeev Kumar, C. L. Chen, C. L. Dong, Y. K. Ho, J. F. Lee, T. S. Chan, R. Thangavel, T. K. Chen, B. H. Mok, S. M. Rao, M. K. Wu, J. Alloys Compd. **554**, 357 (2013).
[3] B. Poornaprakash, P. T. Poojitha, U. Chalapathi, S. Ramu, R. P. Vijayalakshmi, Park Si-Hyun, Ceram. Int. **42**, 8092 (2016).
[4] Lu Wang, Peng Wang, Baibiao Huang, M. Xiaojuan, Gang Wang, Ying Dai, Xiaoyang Zhang, Xiaoyan Qin, Appl. Surf. Sci. **391**, 557 (2017).
[5] Gang-Juan Lee, Sambandam Anandan, Susan J. Masten and Jerry J. Wu, Renew. Energ. **89**, 18 (2016).
[6] Parastoo Bakhtkhosh, Ali Mehrizad, J. Mol. Liq. **240**, 65 (2017).
[7] B. Poornaprakash, U. Chalapathi, Si-Hyun Park, J. Mater. Sci. - Mater. Electron. **28**, 3672 (2017).
[8] B. Poornaprakash, U. Chalapathi, Maddaka Reddeppa, Si-Hyun Park, Superlattices Microstruct. **97**, 104 (2016).

[9] B. Poornaprakash, P. T. Poojitha, U. Chalapathi, Si-Hyun Park, Mater. Lett. **181**, 227 (2016).
[10] B. Poornaprakash, S. Ramu, Si-Hyun Park, R. P. Vijayalakshmi, B. K. Reddy, Mater. Lett. **164**, 104 (2016).
[11] B. Poornaprakash, U. Chalapathi, Mirgender Kumar, P. T. Poojitha, Mater. Sci. - Mater. Electron. **29**, 2316 (2018).
[12] B. Poornaprakash, U. Chalapathi, M. Chandra Sekhar, V. Rajendar, S. V. Prabhakar Vattikuti, M. Siva Pratap Reddy, Youngsuk Suh, Si-Hyun Park, Superlattices Microstruct. **123**, 154 (2018).
[13] B. Poornaprakash, U. Chalapathi, B. Purusottam Reddy, S. V. Prabhakar Vattikuti, M. Siva Pratap Reddy, Si-Hyun Park, Mater. Res. Express **5**, 035018 (2018).
[14] B. Poornaprakash, U. Chalapathi, Youngsuk Suh, Prabhakar S. V. Vattikuti, M. Siva Pratap Reddy, Si-Hyun Park, Ceram. Int. **44**, 11724 (2018).
[15] B. Poornaprakash, U. Chalapathi, B. Purusottam Reddy, P. T. Poojitha, Si-Hyun Park, J. Alloys Compd. **705**, 51-57.
[16] B. Poornaprakash, S. Sambasivam, D. Amaranatha Reddy, G. Murali, R. P. Vijayalakshmi, B. K. Reddy, Ceram. Int. **40**, 2677 (2014).
[17] B. Poornaprakash, D. Amaranatha Reddy, G. Murali, N. Madhusudhana Rao, R. P. Vijayalakshmi, B. K. Reddy, J. Alloys Compd. **577**, 79 (2013).
[18] T. Kushida, A. Kurita, M. Watanabe, Y. Kanematsu, K. Hirata, N. Okubo, Y. Kanemitsu, J. Lumin. **87-89**, 466 (2000).
[19] M. Chandra Sekhar, U. Chalapathi, V. K. Madhu Smitha, P. T. Poojitha, S. Uthanna, B. Poornaprakash, J. Supercond. Nov Magn. **30**, 1937 (2017).
[20] Younes Hanifehpour, Behzad Soltani, Ali Reza Amani-Ghadim, Behnam Hedayati, Bamin Khomami, Sang Woo Joo, Mater. Res. Bull. **76** 411 (2016).